International Journal of Solids and Structures 46 (2009) 1925–1936

Contents lists available at ScienceDirect

International Journal of Solids and Structures

journal homepage: www.elsevier.com/locate/ijsolstr

Stability and size-dependency of Cauchy–Born hypothesis in three-dimensional applications

A. Aghaei, M.J. Abdolhosseini Qomi, M.T. Kazemi, A.R. Khoei *

Center of Excellence in Structural and Earthquake Engineering, Department of Civil Engineering, Sharif University of Technology, P.O. Box 11365-9313, Tehran, Iran

ARTICLE INFO

Article history:
Received 12 August 2008
Received in revised form 9 November 2008
Available online 24 January 2009

Keywords:
Cauchy–Born hypothesis
Validity surface
Size effect
Molecular dynamics

ABSTRACT

The Cauchy–Born hypothesis (CB) provides a hierarchical approach in the molecular theory of crystal elasticity to relate the continuum and atomic deformations. This kinematic theory has been extensively used as the constitutive law of continuum regions in multi-scale models. In these models, the fine scale is proposed to describe the real behavior of crystalline structure wherever the continuum description fails. The main objective of this article is to investigate the stability and size-dependency of CB hypothesis in three-dimensional applications by direct comparison of information between atomistic and continuous description of a medium. The Sutton–Chen many-body potential is used for the gold metal to consider the real metallic behavior in numerical simulations. Two failure criteria are introduced in the strain and stress domains; the validity surfaces are derived for the Cauchy–Born hypothesis; and the size effect of specimens is investigated on the convergency of results. It is shown that the gold crystal deforms homogeneously inside the validity surface, in which the material is elastic and the CB has remained valid. It is observed that although the deformation is inhomogeneous and the CB is invalid outside the validity surface, the crystalline structure may exhibit elastic or plastic behavior in this region. Moreover, it is numerically shown that the size-dependency of validity surface decreases with the increase of the size of specimens. These observations are meticulously investigated by loading and unloading several cubic specimens using molecular dynamics simulation.

1. Introduction

Nanomechanics is encouraging the scientific community, as an emerging branch of nanotechnology, to model, analyze, design and fabricate physical systems at nano-scale. In order to achieve these objectives, researchers have taken the advantage of several approaches, which are classified into the analytical approach (Yoshimoto et al., 2005), computational method (Srivastava and Atluri, 2002), and experimental technique (Domke and Radmacher, 1998). Since the length and the time scales have shrunk to nanometer and nanoseconds, the cost of experimental methods has become absolutely prohibitive. Therefore, the role of analytical and computational methods has been highlighted to mitigate the excessive expenditure on expensive experiments. Due to the arbitrary form of boundaries and facile implementation of boundary conditions in the boundary value problems, the computational methods have been increasingly become popular in scientific communities. Among various methodologies used in computational nanomechanics, the finite element method (FEM) (Huang and Pelegri, 2007), the molecular dynamics (MD) (Horstemeyer et al., 2001) and the multi-scale analysis (Xiao and Belytschko, 2004) are the most popular approaches. The constitutive model which is used in FEM and multi-scale methods is usually based on the Cauchy–Born (CB) hypothesis which is fairly described by Park and Liu (2004).

The Cauchy–Born (CB) hypothesis is a broadly used homogenization theory which stems from the early works of Born and Huang (1962) and then Ericksen et al. (1984). This hypothesis seeks the intrinsic characteristics of material via the atomistic information and can be easily embedded in the classical continuum model. Xiao and Yang (2006) demonstrated that in the Cauchy–Born hypothesis, the implemented deformations must be small enough to prevent the formation of voids and dislocations in the specimens. They expressed that when the solid state materials are subjected to a small loading, the crystalline lattice is stable and thus the CB is valid until the solid-to-solid phase transformation occurs. In addition, they presented that all crystalline materials show this transformation when the underlying crystalline structure becomes unstable at a specific thermo-mechanical load. Elliott et al. (2006) illustrated that after this transformation the lattice reconfigures into a new inhomogeneous stable structure, however – they have not defined a clear statement for this small deformation. Consequently, it is inferred that the CB hypothesis is valid only in particular parts of the strain and stress spaces since it corresponds to homogeneous deformation of crystalline structures.

* Corresponding author. Tel.: +98 21 6600 5818; fax: +98 21 6601 4828.
E-mail address: arkhoei@sharif.edu (A.R. Khoei).

0020-7683/$ - see front matter © 2009 Elsevier Ltd. All rights reserved.
doi:10.1016/j.ijsolstr.2009.01.013

The necessity of introducing an explicit criterion for the validity of CB hypothesis is ingrained by its numerical applications. In the mechanical response of nanostructures via the FE method based on CB hypothesis (Sauer and Li, 2007), the researchers need to assess whether they have acquired authenticated results or not? In addition, the CB hypothesis has been prevalently used as the constitutive law in the continuous part of multi-scale analyses, e.g. quasi-continuum method (Tadmor et al., 1996), bridging domain (Xiao and Belytschko, 2004) and bridging scale method (Liu et al., 2004). These methods were introduced to mitigate the inaccuracy of CB hypothesis wherever the atomic configuration reconfigures to an inhomogeneous structure. In these approaches, a finer scale such as molecular dynamics method was used, however – it was not clearly specified that under which strain or stress state the continuum description fails and the atomistic resolution necessitates. Moreover, in the quasi-continuum method which incorporates an adaptive procedure to specify the atomic scale region, the remeshing criterion is not defined. Thus, the quantification of CB validity for each material in the stress and strain domains is absolutely necessary for the FEM and multi-scale analyses.

The validity of this kinematic hypothesis has been investigated by means of mathematical and comparative approaches by various researchers. Based on the elastic stiffness coefficients, computed by molecular dynamics simulation, Wang et al. (1993) derived a new stability criterion. Their analysis merely checked the crystal instability in uniaxial tension, pure dilatation and thermal loadings. Using the concept of Γ-convergence, Braides et al. (1999) studied the atomistic models and proved the certain discrete functions with pair-wise interaction converge to a continuum model. Friesecke and Theil (2002) proposed the 2D cubic lattice with harmonic springs between nearest and diagonal neighbors to mathematically inquire into the validity of CB. Their solution respected the law of frame-indifference and the spring constants were therefore determined by means of pair inter-atomic potentials. Steinmann et al. (2007) introduced atomistic and continuum failure criteria by using the Lennard–Jones pair potential and studied the validity of CB in two-dimensional lattices subjected to tension and shear deformations. They used the notion of loss of infinitesimal rank 1 convexity at the continuous medium to introduce a continuum failure criterion. Also, they compared the CB deformation with the molecular dynamics simulation to describe the atomistic failure criterion. The above mentioned works deliberated the validity of CB in a few specific loading paths and did not propose the validity surfaces in strain and stress domains. Recently, Khoei et al. (2009) introduced two failure criteria in the strain and stress domains to acquire the validity curves for two-dimensional F.C.C. lattices. The resultant curves for the CB hypothesis were similar to the yield surfaces. The Sutton–Chen many-body potential was used to consider the metallic behaviors of the gold prototype. The above comparative approaches were merely two-dimensional investigations of this issue. In three-dimensional material behavior at nano-scale, the available responses indicate a strong correlation between the material properties and the size of the specimen.

The size-dependency of the prototype is an important issue and has a crucial effect on the result obtained by computational nanomechanics. In general, the surface and interface atoms are exposed to different local environment than counterpart bulk atoms. Duana et al. (2005) investigated that due to different electron density of surface particles, the equilibrium configuration and energy are different from interior atoms. The influence of size-dependency is affiliated to surface-to-volume ratio of the specimen. Typically, for structures with the length more than one hundred nanometers at each side, this ratio is so small and therefore the surface effect is quite negligible. Thus for these structures, the elastic behavior of the structure is governed by the bulk properties (Sharma et al., 2003), i.e. the Young modulus and Poisson ratio (Malvern, 1968). This effect is demonstrated in experimental observations (Wong et al., 1997), analytical analyses (Salacuse et al., 1996) and numerical simulations (Miller and Shenoy, 2000). Streitz et al. (1994) and He et al. (2004) investigated the size-dependency of thin films by means of molecular dynamics and analytical methods, respectively. Zhou and Huang (2004) proposed a combination of molecular statics and ab initio calculations to demonstrate that a solid surface can be either softer, or stiffer elastically than the corresponding bulk for different nano-structures. Dingreville et al. (2005) developed a framework to incorporate the surface free energy into the continuum theory of mechanics. They demonstrated that the overall elastic behavior of nano-particles, nanowires and thin films are size-dependent. Using molecular dynamics simulations, the size and strain rate effects in simple shear deformation are investigated on the mechanical responses of F.C.C. metals by Guo et al. (2007). Fleck and Hutchinson (1993) and Gao and Huang (2003) indicated the importance of geometrically necessary dislocations and included the material length scale into the strain gradient plasticity theory. Despite of these extensive researches on the size effect, to the knowledge of authors, no research works have been done on the size-dependency of Cauchy–Born hypothesis.

In the present work, the size-dependency and the validity of CB hypothesis in three-dimensional latticed structures are studied by comparatively analyzing the results of continuum mechanic calculations and the molecular dynamics simulations. The Sutton–Chen many-body potential is proposed to model the real metallic behaviors of gold single crystalline structures. By implementation of different deformation paths to the samples with different sizes, such as the shear and triaxial deformations, the validity surfaces are derived. These convex surfaces are intuitively similar to the yield surfaces in theory of plasticity, in which the material exhibits the elastic deformation inside of surfaces. Although the material undergoes unrecoverable deformation outside of the yield surface in plastic region, it is numerically shown that the material undergoes inhomogeneous but recoverable deformation in some regions outside the CB validity surface. In Section 2, a concise description of the Cauchy–Born hypothesis is provided along with the calculation of stress in a continuum based on CB. Section 3 provides the basic prerequisites of classical molecular dynamics simulation. Subsequently, two failure criteria are defined in the stress and strain domains. The results and discussions over several molecular dynamics simulations are given in Section 4. The validity surfaces are provided and their dependency on the size effect is discussed in this section. Finally, some concluding remarks are given in Section 5.

2. Cauchy–Born hypothesis

The Cauchy—Born (CB) hypothesis is a hierarchical assumption for modeling the elastic behavior of material at atomic scale. In CB hypothesis, the atomic configuration is affiliated to the continuum deformation by means of the local deformation gradient, as shown in Fig. 1 (Tadmor et al., 1996; Sunyk and Steinmann, 2003). The deformation gradient tensor F_{ij} enables the relative spatial position of two neighboring particles after the deformation, which has been described in terms of their relative material position before the deformation. Malvern (1968) and Belytschko et al. (2000) explicitly expressed that by considering an infinitesimal line segment dX_i in the reference configuration, the corresponding line segment dx_i in the current configuration is given by

$$dx_i = F_{ij} dX_j \tag{1}$$

where i and j denote the Cartesian directions. In CB hypothesis, the lattice vectors are considered as infinitesimal vectors. This assumption leads to a mathematical approximation since the lattice vectors

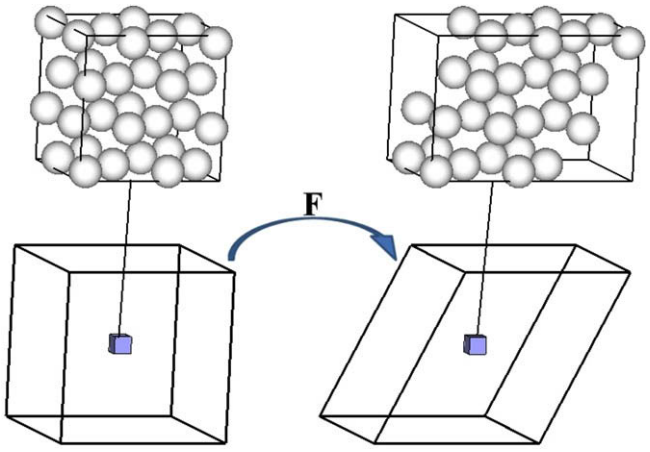

Fig. 1. The CB hypothesis; the deformation of atoms conforms to the deformation of continuous medium.

have finite lengths. Therefore, the accuracy of CB decreases consequently by increasing the deformation of the lattice. This rule is applicable, as long as the crystal deformation is nearly homogeneous in the scale of the lattice vectors (Guo et al., 2006).

In hyperelasticity, the stress tensor can be derived by differentiating the strain energy density w_0 of the deformed material with respect to its conjugate strain measure. Calculating the strain energy density w_0 from the CB hypothesis in a crystalline body subjected to the deformation gradient F_{ij}, the first Piola–Kirchhoff stress tensor P_{ij} can be calculated as

$$P_{ij} = \frac{\partial w_0}{\partial F_{ij}} \tag{2}$$

Since F_{ij} is not symmetric, the first Piola–Kirchhoff tensor P_{kj} is not a symmetric tensor. Thus, we substitute P_{kj} with the symmetric Cauchy stress tensor as

$$\sigma_{ij} = J^{-1} F_{ik} P_{kj} \tag{3}$$

where J is the determinant of the deformation gradient tensor, called as Jacobian. In nano-scale simulations, the strain energy density can be derived using the inter-atomic potentials. In spite of the simplicity and rational computational expense of the pair-wise potentials, such as the Lennard–Jones and Morse potentials, Ackland and Vitek (1990) have shown that those potentials are incapable of modeling the convexity of the metallic surfaces and cannot correctly illustrate the Cauchy relations for metals, i.e. $C_{12} \neq C_{44}$, where $\boldsymbol{C}$ is the tangent elastic matrix. Therefore, the Sutton–Chen many-body potential is chosen here for the calculation of potential energy (Sutton and Chen, 1990; Rafii-Tabar, 2000). The potential energy of the multi-particle system is defined as

$$\begin{aligned} w_0 = w_{0i} &= \frac{\varepsilon}{\Omega_{0i}} \left[\frac{1}{2} \sum_{j \neq i} V(r_{ij}) - c\sqrt{\rho_i} \right] \qquad \text{where } V(r_{ij}) \\ &= \left(\frac{a}{r_{ij}} \right)^n, \quad \rho_i = \sum_{j \neq i} \left(\frac{a}{r_{ij}} \right)^m \end{aligned} \tag{4}$$

where Ω_{0i} is the local atomic volume in the relaxed and undeformed configuration of the latticed structure associated with the atom i, w_{0i} is the potential energy density of the atom i, r_{ij} is the inter-atomic distance between the host atom i and its neighbor j, a is the lattice parameter and m, n, c and ε are the potential parameters. These constants are obtained for ten different FCC metals by Sutton and Chen (1990).

Using Eqs. (2)–(4) and considering that the Jacobian is the ratio of an infinitesimal volume in the deformed body to the corresponding volume of that body in undeformed configuration, the Cauchy stress tensor at the atomic site can be derived as

$$\sigma_i^{\alpha\beta} = \frac{-\varepsilon}{2\Omega_i} \sum_{j \neq i} \left[n \frac{a^n}{r_{ij}^{n+2}} - \frac{cm}{2} \left(\frac{1}{\sqrt{\rho_i}} + \frac{1}{\sqrt{\rho_j}} \right) \frac{a^m}{r_{ij}^{m+2}} \right] r_{ij}^{\alpha} r_{ij}^{\beta} \tag{5}$$

where r_{ij}^{α} is the atomistic distance between the atom i and its neighbor in αth direction and Ω_i is the local atomic volume in the deformed configuration which is identical to the volume of the Voronoi polyhedron associated with the atom i (Rapaport, 1995). Since the CB hypothesis assumes that the underlying lattice, which constructs the body of the continuum, should undergo a homogeneous deformation, the above atomic stress is identical in all atomic sites in the lattice, i.e. $\sigma_{\mathrm{CB}}^{\alpha\beta} = \sigma_i^{\alpha\beta}$.

3. Modeling and simulation of atomistic medium

3.1. Classical molecular dynamics simulation

In this section, the molecular dynamics (MD) method is employed to determine the validity and failure of the Cauchy–Born hypothesis. Since all materials from nano-to-macro scale, are constructed by the atoms or molecules, the atomic structure plays a fundamental role in different modes of material behavior. The classical molecular dynamics is a powerful technique for computing the equilibrium and non-equilibrium characteristics of the materials. The term of 'classical' indicates that the motion of constituent particles obeys the laws of classical mechanics. On the other hand, the MD simulation is a numerical solution of the second Newton law of motion in a step-by-step fashion in time domain. In a multi-particle system, the second order differential equation for the ith atom can be written as

$$\mathbf{f}_i = m_i \ddot{\mathbf{r}}_i \tag{6}$$

where m_i is the mass of ith atom. In order to solve the above equation, the force acting on the ith particle must be calculated. Using the Sutton–Chen potential (Eq. 4) and considering the fact that the Newtonian force exerted on each atom is identical to the derivatives of the total potential energy with respect to the spatial coordinate of the atom, the force can be derived as

$$\mathbf{f}_i^{SC} = -\frac{\varepsilon}{r_{ij}^2} \sum_{j \neq i} \left[n \left(\frac{a}{r_{ij}} \right)^n - \frac{mc}{2} \left(\frac{1}{\sqrt{\rho_i}} + \frac{1}{\sqrt{\rho_j}} \right) \left(\frac{a}{r_{ij}} \right)^m \right] \mathbf{r}_{ij} \tag{7}$$

where $\mathbf{r}_{ij}$ is the separation vector between the ith atom and its neighbor j. The equation of motion (Eq. 6) for each degree of freedom can be integrated individually through the time by means of the finite difference method. Thus, the $3N$ coupled differential equations need to be solved in time domain for three-dimensional analyses. In this study, the velocity-Verlet algorithm (Allen and Tildesley, 1987) is utilized, which is the most popular algorithm in MD simulations.

It must be noted that the effect of temperature is excluded here from the validity and failure of CB hypothesis and all MD simulations are performed at zero temperature. Thus, the Berendsen thermostat (Berendsen et al. (1984)) is chosen to maintain the temperature of the system during the simulation. This type of molecular dynamics locally minimizes the total potential energy of multi-particle system. This process is a numerical implementation of the analytical notion presented by Friesecke and Theil (2002), in which the atomic positions predicted by CB hypothesis locally minimize the total potential energy. By implementing the thermostat to the velocity-Verlet algorithm, equation of motion (Eq. 6) transmutes to the following discrete form

$$
\begin{aligned}
&\mathbf{r}_i(t+\Delta t) = \mathbf{r}_i(t) + \mathbf{v}_i(t)\Delta t + \tfrac{1}{2m_i}\Delta t^2 \mathbf{f}_i(t)\\
&\mathbf{v}_i\left(t+\tfrac{1}{2}\Delta t\right) = \mathbf{v}_i(t) + \tfrac{1}{2m_i}\Delta t \mathbf{f}_i(t)\\
&T\left(t+\tfrac{1}{2}\Delta t\right) = \left[\sum_{i=1}^{N} m_i \mathbf{v}_i^2\left(t+\tfrac{1}{2}\Delta t\right)\right] \Big/ 3Nk_B\\
&\mu\left(t+\tfrac{1}{2}\Delta t\right) = \gamma\left[1 - \tfrac{T_o}{T\left(t+\frac{1}{2}\Delta t\right)}\right]\\
&\mathbf{v}_i(t+\Delta t) = \tfrac{2}{2+\mu\left(t+\frac{1}{2}\Delta t\right)\Delta t}\left[\mathbf{v}_i\left(t+\tfrac{1}{2}\Delta t\right) + \tfrac{1}{2m_i}\Delta t \mathbf{f}_i(t+\Delta t)\right]\\
&\mathbf{f}_i(t+\Delta t) = \mathbf{f}_i^{SC}(t+\Delta t) - m_i\mu\left(t+\tfrac{1}{2}\Delta t\right)\mathbf{v}_i(t+\Delta t)
\end{aligned}
\tag{8}
$$

where $\mathbf{r}_i$, $\mathbf{v}_i$ and $\mathbf{f}_i^{SC}$ are the spatial vector, velocity and the internal force calculated by Sutton–Chen potential for ith atom, $\mathbf{f}_i$ is the modified force due to frictional effect for ith atom, T is the instantaneous temperature of the system, T_0 is the reference temperature which is set to zero, γ is a constant factor of the Berendsen thermostat and k_B is the Boltzmann's constant. In 3D analysis, above equations must be solved for $3N$ degrees of freedom, with N denoting the number of atoms.

The validity of CB hypothesis can be investigated by comparing the deformations of the continuous and atomistic (Eq. 8) mediums. Furthermore, it can be evaluated by contrasting the mechanical properties of the specimen in the atomistic and continuous descriptions. For example, the elastic modulus, which plays an important role in the mechanical behavior of the system, can be used for the assessment of validity of the CB hypothesis. Since the strains applied in the boundaries of the atomic and the continuum specimens are identical, the stress measurement may be applied instead of the elastic modulus. Furthermore, since the stress has traditionally been a continuum description, various stress measurements have been defined by researchers to evaluate the atomic stress, including: the Virial stress (Subramaniyan and Sun, 2008), Hardy stress (Zimmerman et al., 2004), Lutsko stress (Shen and Atluri, 2004), etc. Shen and Atluri (2004) demonstrated that the formulation of Cauchy stress described in previous section (Eq. 5) is equivalent to the BDT atomic stress which is defined by Basinski–Duesbery–Taylor. Subramaniyan and Sun (2008) have shown that for those simulations carried out in zero temperature, the Virial stress, BDT stress and Cauchy stress are identical. Since the BDT stress depends merely on the atomic coordinates, all atoms have similar stress in a homogeneously deformed system. A small perturbation in the atomic configuration will change the atomic stresses and thus, each point in the specimen will have different stresses. Thus, it is important to nominate an average stress for the atomic scale, which represents the continuum mechanics stress at the continuum point as

$$
\sigma_{\mathrm{MD}}^{\alpha\beta} = \frac{1}{N}\sum_{i=1}^{N} \sigma_i^{\alpha\beta} \tag{9}
$$

where N denotes the total number of unconstrained atoms, in order to eliminate the effect of surface from the calculated stress. This technique is also used by Horstemeyer et al. (2001).

3.2. Failure criteria

In what follows, two distinct failure criteria are introduced in the strain and stress domains to appraise the validity of CB hypothesis. As mentioned earlier, this procedure is performed by the direct comparison between the coordinates of particles and the stress of the specimen in continuum and atomic fields due to a perturbation in the homogeneous system. In other words, after exerting a uniform deformation to atoms on the boundary, which is completely in accordance with the CB deformation, the remaining internal atoms are set free to lead the system to its local minimum energy, i.e. the configuration which locally minimizes the total energy of the system and essentially is not equal to the deformation predicted by CB. The displacement standard deviation *DSD* is computed as

$$
DSD = \sqrt{\frac{1}{3N-1}\sum_{i=1}^{N}(\mathbf{r}_i^{\mathrm{MD}} - \mathbf{r}_i^{\mathrm{CB}})^2}/a \tag{10}
$$

where N is the total number of the particles whether constrained or not, $\mathbf{r}_i^{\mathrm{MD}}$ and $\mathbf{r}_i^{\mathrm{CB}}$ are the spatial coordinate vectors of ith atom which are computed by means of the MD solution and homogeneous CB deformation, respectively, and a is the lattice parameter. In addition to above formula which evaluates the validity of CB in strain domain, the stress absolute deviation from the Cauchy–Born hypothesis is defined in stress field as

$$
SAD^{\alpha\beta} = |\sigma_{\mathrm{MD}}^{\alpha\beta} - \sigma_{\mathrm{CB}}^{\alpha\beta}| \tag{11}
$$

where $\sigma_{\mathrm{MD}}^{\alpha\beta}$ is the $\alpha\beta$th component of the average of BDT stress tensor derived using the MD simulation (Eq. 9) and $\sigma_{\mathrm{CB}}^{\alpha\beta}$ is the same component of Cauchy stress tensor predicted by means of the CB hypothesis (Eq. 5).

4. Computational analyses and results

In order to investigate the limitation of CB hypothesis in 3D applications, several MD simulations with different sizes and deformation paths were performed. At first stage, the specifications of the specimens and numerical prerequisites are given for MD simulations. Then, the influence of the size effect on the results is investigated. Finally, the validity surface is obtained for the gold metal by applying two specimens to different triaxial deformation paths.

4.1. Numerical details

In order to perform the numerical simulation, seven single crystalline cubic specimens with different sizes are generated in accordance with the ideal geometrical F.C.C. lattice. These specimens are constructed of 1372, 2048, 2916, 4000, 8788, 16384 and 32000 gold atoms. Since the 3D nano-scale specimens have a high ratio of surface-to-volume, the size effect has a significant effect in numerical results. The computational CPU time was really time-consuming in modeling of 5 nanoseconds, and in simulation of the largest specimen took more than seven days with a 2.4-GHz processor. The rectangular coordinate system is employed, and the x, y, and z axes are chosen parallel to the [100], [010], and [001] crystal directions, respectively.

In order to solve the MD equation of motion (Eq. 8) the time step is set to 0.001 dimensionless time. This time step is called micro time step. The dimensionless time for gold metal is 5.1542 picoseconds. The Berendsen thermostat parameter is set to 2, as a constant value during the simulation. The 20,000 micro time steps are carried out for the relaxation procedure. After relaxation phase, two planes of boundary atoms in each side are frozen on their relaxed lattice site (Fig. 2). The cut-off radius includes the third neighbors into the calculations. The boundary displacement in MD simulation which is identical to CB deformation is divided into 200 identical portions. One portion is implemented at each macro time step, which consists of 5000 micro time steps. In the first micro time step of each macro time step, the portion of deformation according to CB hypothesis is implemented over all boundary atoms, in which they retain this deformation during the macro time step. The rest of atoms are released to reach a position which locally minimizes the total potential energy of the multi-particle system.

Since all simulations are performed based on the displacement-control technique, the effect of Poisson ratio merely contributes to

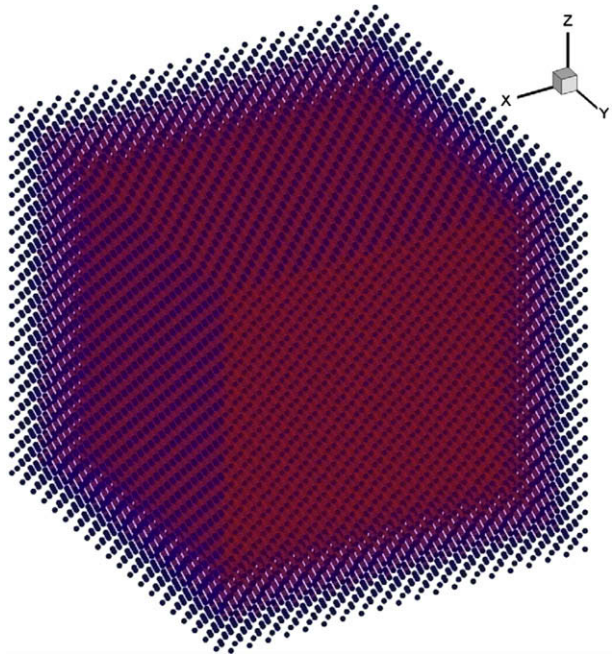

Fig. 2. The specimen with 32,000 atoms. The boundary atoms (blue) are frozen during each macro time step and follow the CB deformation. Coordinate of the red atoms are computed via the MD simulation. (For interpretation of color mentioned in this figure the reader is referred to the web version of the article.)

the adjustment of location of internal atoms, and as a result, it implicitly engages in the calculation of atomic stresses. For instance, by extending one side of a specimen the stress subsequently increases in the other directions. It must be noted that the displacement-control technique is used here to reflect the concept of CB hypothesis which predicts the atomic positions according to an arbitrary deformation gradient, and it does not violate the basic principles of solid mechanics. Finally, the results of *DSD* and *SAD* are computed at the last micro time step of each macro time step. All simulations are performed by MASS software which has been developed by the authors (for further details of the software readers are referred to www.nano-mass.com).

4.2. Effect of size-dependency

4.2.1. Simple shear

In simple shear deformation, the deformation gradient tensor is defined as

$$\mathbf{F} = \begin{bmatrix} 1 & \tan\theta & 0 \\ 0 & 1 & 0 \\ 0 & 0 & 1 \end{bmatrix} = \begin{bmatrix} 1 & \alpha & 0 \\ 0 & 1 & 0 \\ 0 & 0 & 1 \end{bmatrix} \tag{12}$$

where α and θ represent the shear number and shear angle, respectively. All seven specimens are subjected to the simple shear deformation and the final shear number is set to 0.22. The break point of CB hypothesis is defined by the point that dislocations are emitted in the specimen and thus, the values of *DSD* and *SAD* increase intensively. In Fig. 3, the initiation of dislocations is shown together with the behavior of specimen and its break point. Figs. 4(a) and (b) present the variation of *DSD* versus shear strain and the trend of *SAD* versus CB stress, respectively. In Figs. 5(a) and (b), the convergences of the stress and strain are demonstrated at the break points. In 3D simulation, the magnitudes of the deviations are less than two-dimensional analyses derived by Khoei et al. (2009). For example, the ratios of the converged *DSD* and *SAD* at the break points in 2D and 3D analyses are as follows:

$$\frac{DSD_{2D}}{DSD_{3D}} = 2.07$$
$$\frac{(SAD/CB_{stress})_{2D}}{(SAD/CB_{stress})_{3D}} = 4.31$$

As can be seen from Fig. 4(b), the larger specimens have smaller stress deviations for the CB stress less than 2.4 GPa. This trend is reversed for the CB stress between 2.4 and 9 GPa, where the larger specimens have larger deviations. For the CB stress greater than 9 GPa, this trend begins to reverse, and as a result, the larger specimen begin to have smaller stress deviations. This process is fully accomplished for specimens up to 7888-atoms, however – the larger specimens have broken down before completing the inversion process. It can be therefore highlighted that the stress deviation of specimen is minimal at the yield point of specimen with 7888-atoms. It must be noted that the shear stress deviations are less than 0.8% of the average BDT stress which is absolutely negligible with respect to 5% deviation of shear stress reported in 2D analyses by Khoei et al. (2009). Fig. 4(c) illustrates the shear stress–shear number curve for all specimens. Comparing Figs. 4(a) and (c), we can conclude that in shear deformation the break point of CB coincides with the yield point of the material.

4.2.2. Uniaxial tension and compression

In three-dimensional classical continuum mechanics, the uniform uniaxial deformation is given by

$$\mathbf{F} = \begin{bmatrix} \partial x/\partial X & 0 & 0 \\ 0 & 1 & 0 \\ 0 & 0 & 1 \end{bmatrix} = \begin{bmatrix} \lambda & 0 & 0 \\ 0 & 1 & 0 \\ 0 & 0 & 1 \end{bmatrix} \tag{13}$$

in which λ is analogous to the magnitude of the uniaxial deformation divided by the initial length of the specimen (stretch). If $\lambda > 1$, it represents the tensile strain and $\lambda < 1$ if it is the compressive strain. The uniaxial strain is equal $\lambda - 1$ to which is similar to the first component of Green strain tensor. In order to investigate the size effect of the specimens, the samples with different sizes are subjected to compression and tension deformation paths. In Fig. 6(a), the variation of *DSD* is plotted with the uniaxial strain. As can be seen from this figure, the size effect has a negligible effect on the tension results, i.e. all samples are broken in about 10% strain. In fact, similar to shear deformation, all specimens subjected to extension have an identical CB break point with the yield point of material. This can be inferred by comparing Fig. 6(a) with the yield points of strain–stress curve in tensile loading (Fig. 7a).

On the contrary, the compressive samples exhibit some complex behavior and have more dependency on the size of specimens. It can be observed that although there is one break point in the stress–strain diagram, as shown in Fig. 7(b), there can be seen three distinct break points in the strain domain and one break point in the stress domain in compression region, as shown in Figs. 6(a) and (c), respectively. It is apparent that the CB hypothesis fails at the first break point of *DSD* diagram, however – it is not clear that in which point the material has been yielded. In order to determine the material yield point, the specimen with 8788-atoms is unloaded from four distinct points, as shown in Fig. 8. In this figure, the evolution of *DSD* is presented for the loading process together with unloading process from four distinct points. Although the unloading process from the first point has been crossed by the loading process, the second and third unloading experiments produce a hysteresis behavior in which the loaded specimen procrastinate its reconfiguration to the homogeneous deformation. On the other hand, the unloading process of second

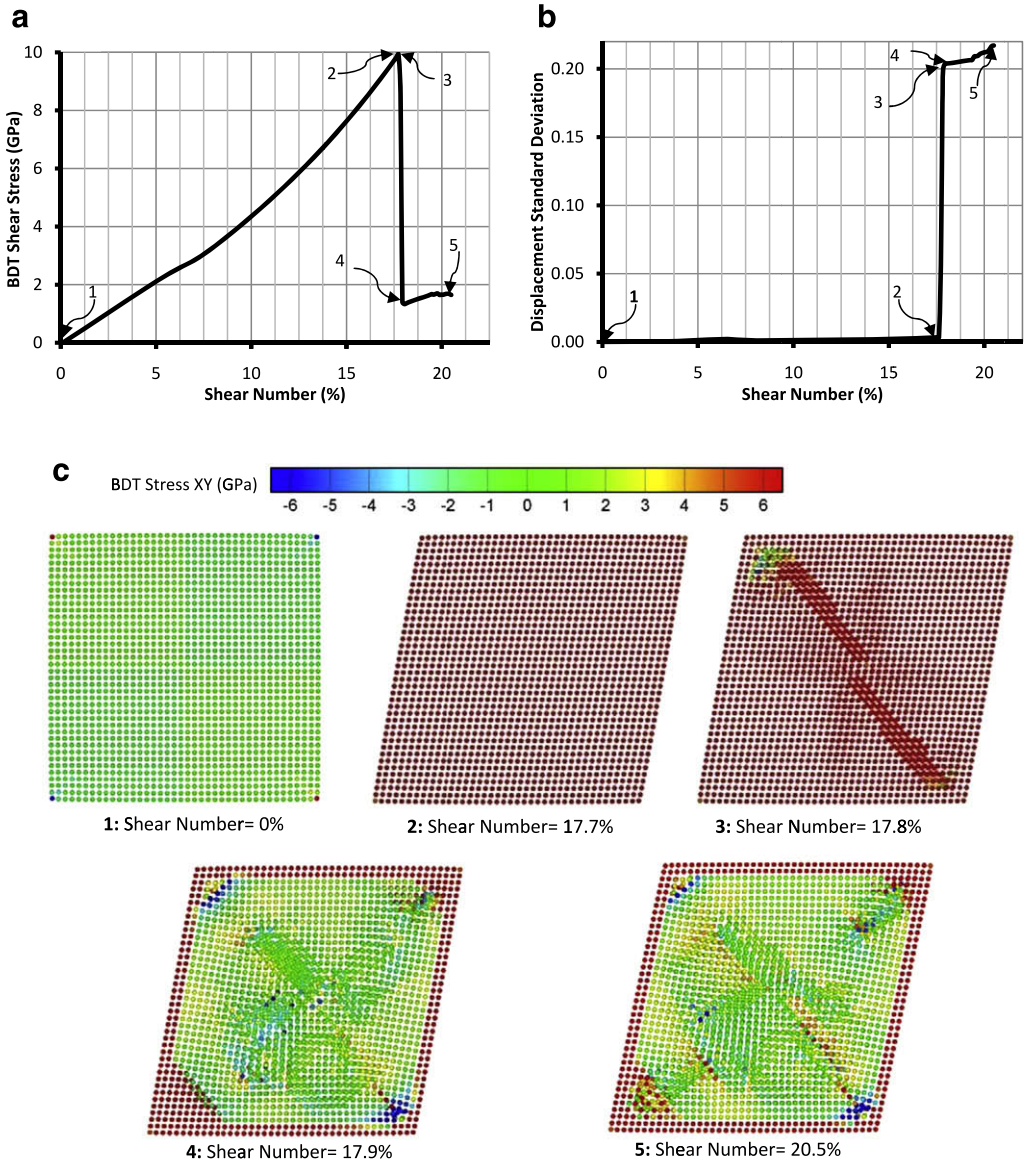

Fig. 3. (a) The shear stress–shear number curve, (b) the *SAD*-shear number curves for the 32,000-atom specimen, (c) the evolution of the atomic positions during the simulation. (The Cauchy–Born fails at the third level.)

and third points did not exactly pass through the loading process, and more deformation was needed to lead the specimen to a homogeneous configuration. The reason behind the evolution of the hysteresis phenomenon is mainly due to the inherent characteristic of solution of the multi-particle systems at zero temperature. As mentioned earlier, the damped MD simulation is equivalent to the energy minimization process. In such a model, the system leads to its minimal potential energy by implementing certain constraints and providing the system with sufficient relaxation time. Basically, we need to clarify two main facts here; Firstly, by the MD simulation we obtain a configuration which *locally* minimizes the total potential energy of the system, but the system may have numerous minimal points in phase space. Indeed, this minimal point depends on the position of the phase space point, e.g. the atomic configuration. If the temperature is close to zero, the system may be tangled in one local minimum, and more energy is therefore needed to push the system out of this minimum. This is the main reason for justification of hysteresis phenomenon. Secondly, the simulation of multi-particle systems in canonical ensemble via Brendsen thermostat makes the simulation irreversible. In fact, because the Brendsen formulation fails to work appropriately at zero temperature, the temperature must be set to a negligible value. As a result, the system may not exactly return to its initial geometry, and minuscule perturbations are inevitable. In this way, in the unloading process from the second or third break points, the system does not return to the initial relaxed configuration, however – it cannot be concluded that the system undergoes the plastic deformation. Close inspection of the specimen revealed that no dislocations have been emitted in the system, and after complete unloading all stress tensor components were uniformly zero for internal atoms. Therefore, in the first and second break points the material is still elastic, and if the specimen is unloaded, the atoms almost return to their initial positions. However, the specimen does not return to its initial configuration if it is unloaded from the third break point, which expresses that the plastic regime starts from this point.

By contrasting Figs. 6 and 7, it can be inferred that the material yield point coincides with the break point of *SAD* diagram, in which

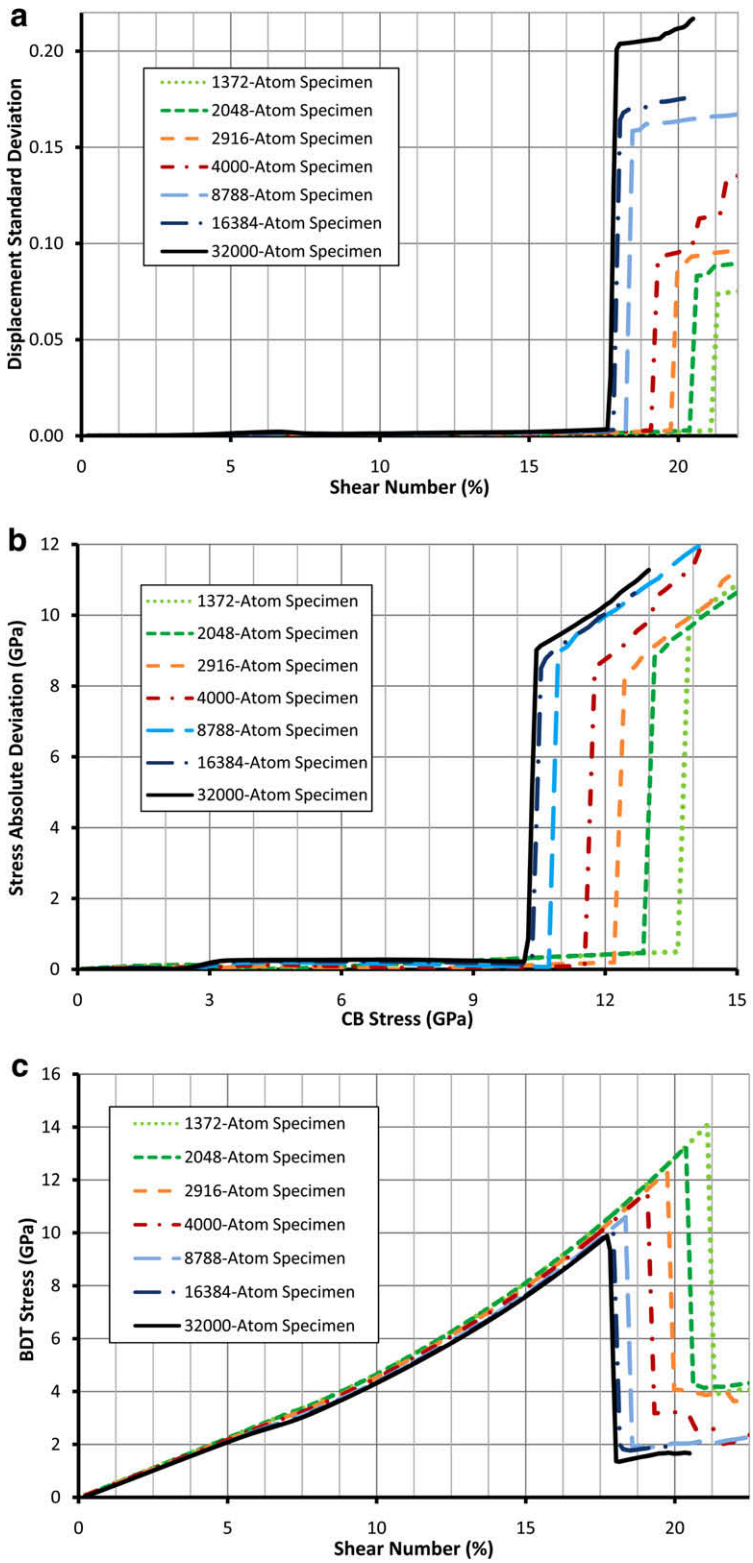

Fig. 4. The simple shear deformation. (a) Evolution of DSD versus shear number; (b) evolution of shear component of *SAD* versus shear stress; (c) shear stress–shear number curve.

these two points occur simultaneously with the last break point of *DSD* diagram. Thus, the *SAD* break point does not pertain to the CB failure and it is related to the material yield point. Fig. 6(a) illustrates that in compression region, the small samples (samples with 1372 and 2048-atoms) have two break points and undergo more strain in contrast with the larger specimens. In fact, the CB hypothesis is more valid in smaller specimens. In the largest specimen, the behavior of *DSD* diagram after the first break point does not comply with the behavior of the smaller samples. In Figs. 4(a) and (b), the convergences of the stress and strain are illustrated at break points with increasing the number of atoms. By comparing the results in tension and compression, it can be easily deduced that the

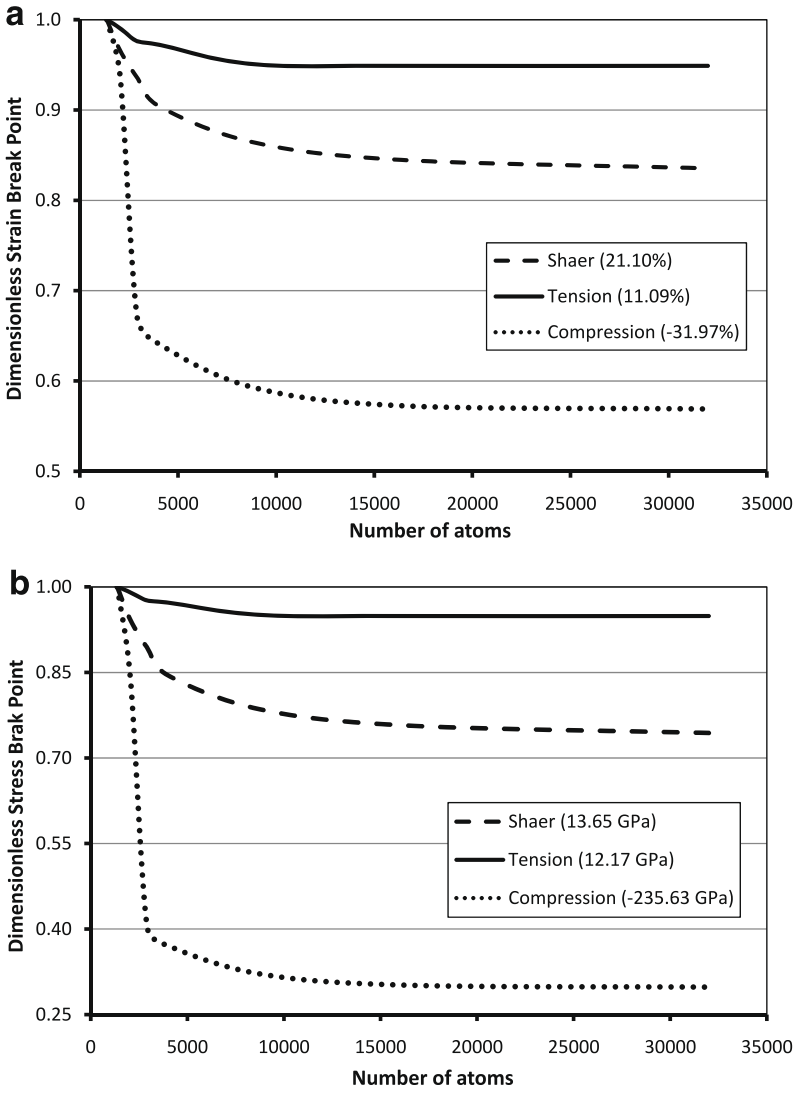

Fig. 5. The convergency of (a) strain and (b) stress at the break points versus the size of the samples. All values are divided to the maximum value of the corresponding curve to make them dimensionless. The numbers in the parentheses show the maximum value of the curves.

material is much more stable in both strain and stress domains and thus, the CB is more valid in compression rather than tension.

Comparing the 2D result reported by Khoei et al. (2009) with the current 3D analyzes, we can conclude that the value of the deviations of strain domain in three-dimensional simulation is more than two-dimensional analysis, but it is less in the stress domain. For instance, the ratios of the converged *DSD* and *SAD* at the break points in 2D and 3D analyzes are

$$\frac{DSD_{2D}}{DSD_{3D}} = \begin{cases} 0.26; & \textit{Tension} \\ 0.79; & \textit{Compression} \end{cases}$$

$$\frac{(SAD/CB_{stress})_{2D}}{(SAD/CB_{stress})_{3D}} = \begin{cases} 1.91; & \textit{Tension} \\ 13.1; & \textit{Compression} \end{cases}$$

4.3. Triaxial tests and the validity surface

In order to obtain a validity surface and observe the size-dependency of Cauchy–Born hypothesis, two specimens with 1372 and 4000 atoms were subjected to various combination of strains in *x*, *y* and *z* directions. The *DSD*, *SAD* and stress–strain curves of each simulation are plotted and the strain and stress states corresponding to the first break point are determined. On the virtue of symmetry of cubic specimens, each break point represents 6 points in three-dimensional space. Hence, if the specimen fails at point $(\varepsilon_x, \varepsilon_y, \varepsilon_z)$ in the strain domain, where ε_x denotes the axial strain in *x*-direction, it will also fail at point $(\varepsilon_y, \varepsilon_z, \varepsilon_x)$. So by performing 12 experiments, we can provide 72 break points for each specimen in the strain and stress domains. By taking the advantage of a simple computational geometry algorithm for indicating the nearest vertices of the obtained points of the validity surface, we are able to visualize the surface in three-dimensional strain space. The validity surfaces of two specimens are plotted in the strain space, as shown in Fig. 9.

Fig. 9 indicates that the validity surface becomes smaller for the larger specimen. As discussed in previous sections, the size-dependency of results can be overcome by increasing the size of specimen. The validity surface is a simply-connected and convex surface. The CB hypothesis is valid and the material is elastic inside the surface. The CB is invalid outside the surface and the crystalline material can experience either elastic or plastic deformation. In other words, in some portion of the outside space

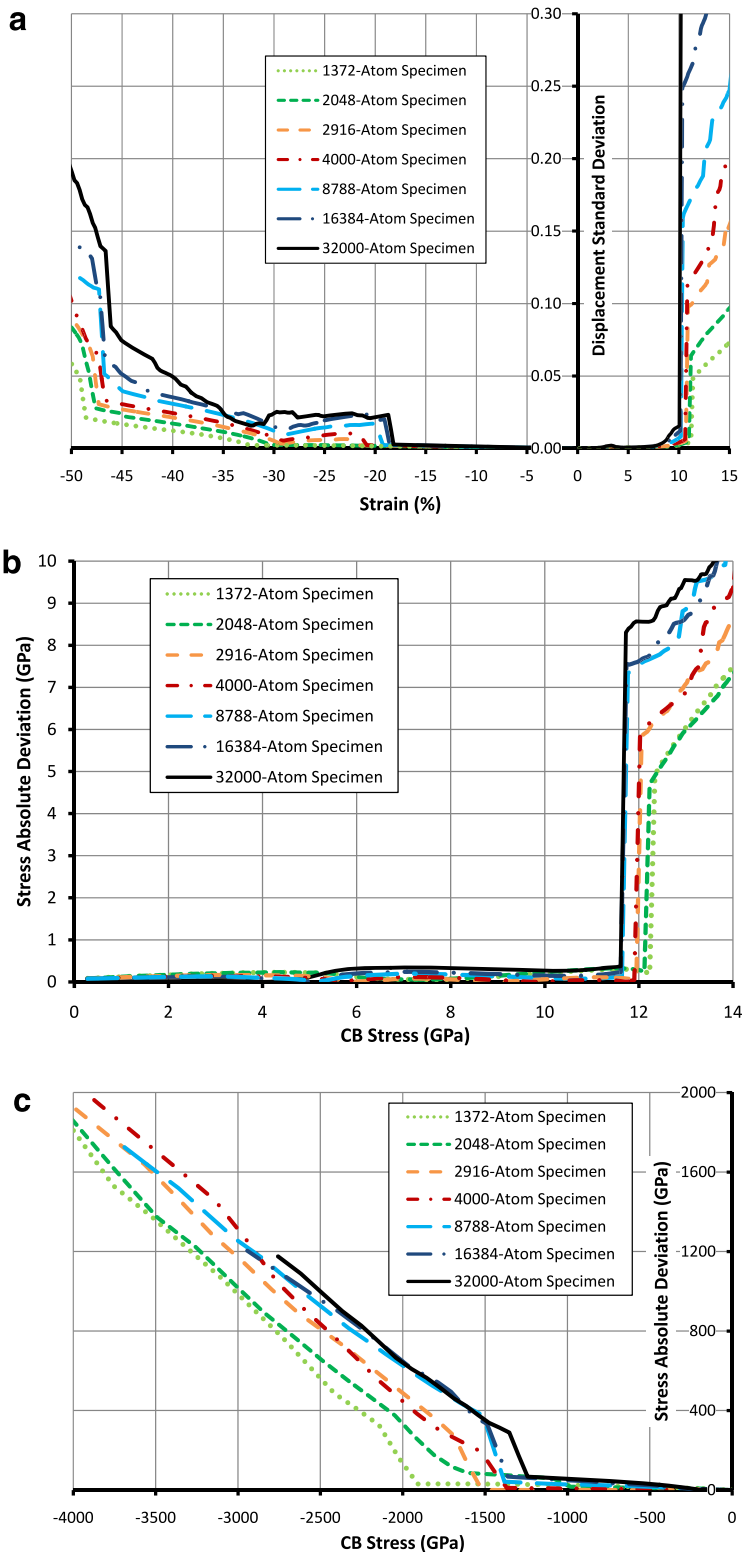

Fig. 6. Uniaxial deformation. (a) evolution of DSD versus uniaxial strain; (b) evolution of *SAD* versus uniaxial tension; (c) evolution of *SAD* versus uniaxial compression.

of the validity surface (not in all parts), the material is experiencing inhomogeneous deformation which is recoverable. Further investigations on the molecular dynamics specimens revealed that in these parts of strain space, the strain energy accumulated in the latticed structure is not enough for the initiation of dislocations, and the material therefore exhibits the elastic behavior.

As a practical guideline, we introduce here the equation of validity surface in the strain domain. Using a simple search algorithm which minimizes the curve fitting error, the constant variables are calibrated for 1372-atom and 4000-atom specimens. The validity surface equation is given by

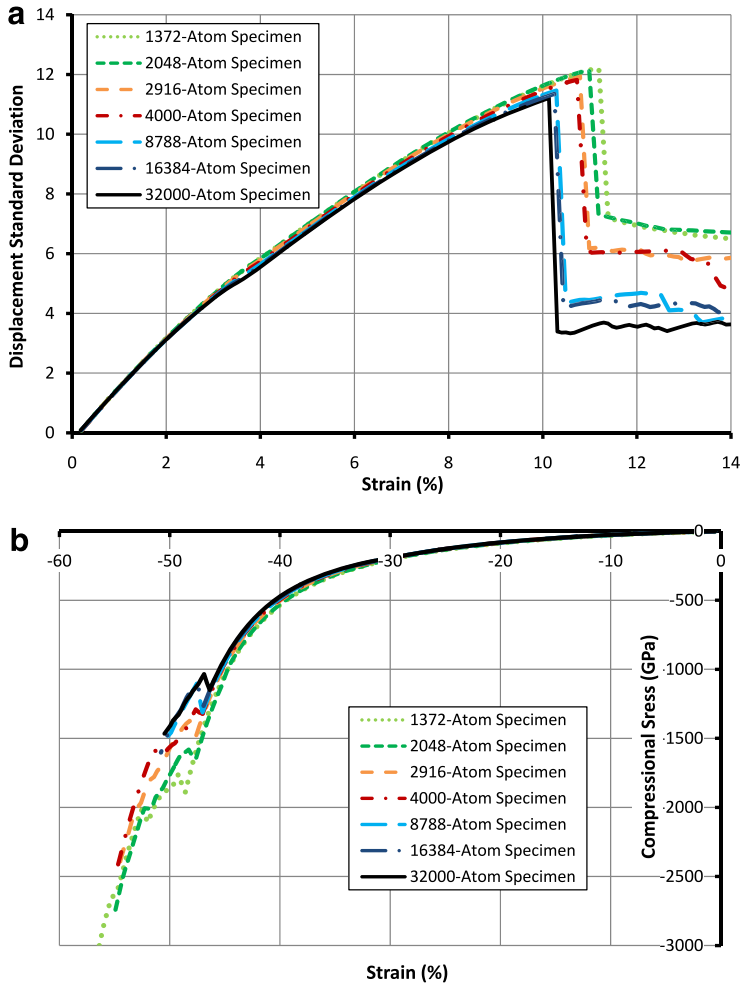

Fig. 7. Uniaxial deformation. (a) Tensile stress versus tensile strain, (b) compressive stress versus compressive strain.

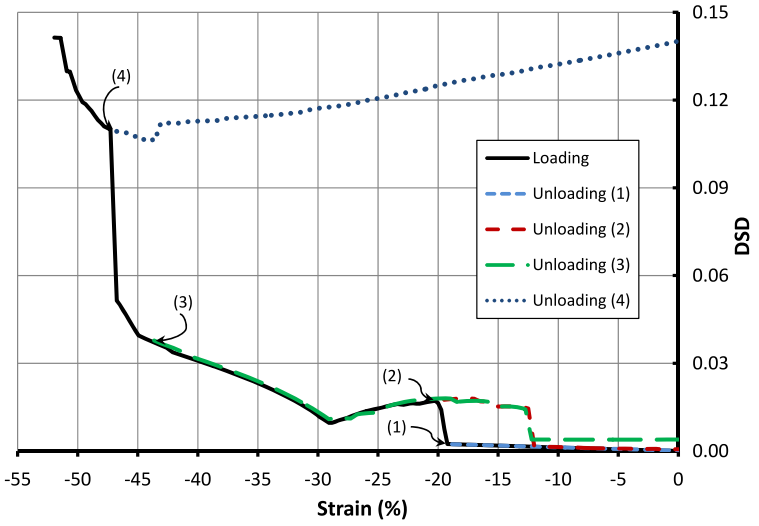

Fig. 8. The DSD versus compressive strain for unloading process of 8788-atom specimen. The specimen is unloaded from four levels. The first and second levels are before and after the first break point of CB hypothesis, respectively. The third and forth levels are before and after the third break point of CB hypothesis, respectively.

$$\left\{A\left(B\frac{\rho}{\varepsilon_c}+C\frac{\varepsilon_V}{\varepsilon_c}\right)^2+D\frac{\rho}{\varepsilon_c}\right\}^2+m_0\left[B\frac{\rho}{\varepsilon_c}r(\cos(\theta))+C\frac{\varepsilon_V}{\varepsilon_c}\right]=1 \qquad (14)$$

where ε_V and γ are the volumetric and deviatoric strains, respectively, defined as and $\varepsilon_V=(\varepsilon_x+\varepsilon_y+\varepsilon_z)/3$, $\gamma_x=\varepsilon_x-\varepsilon_V$, with $\varepsilon_x,\varepsilon_y,\varepsilon_z$ denoting the principal strains. In above relations,

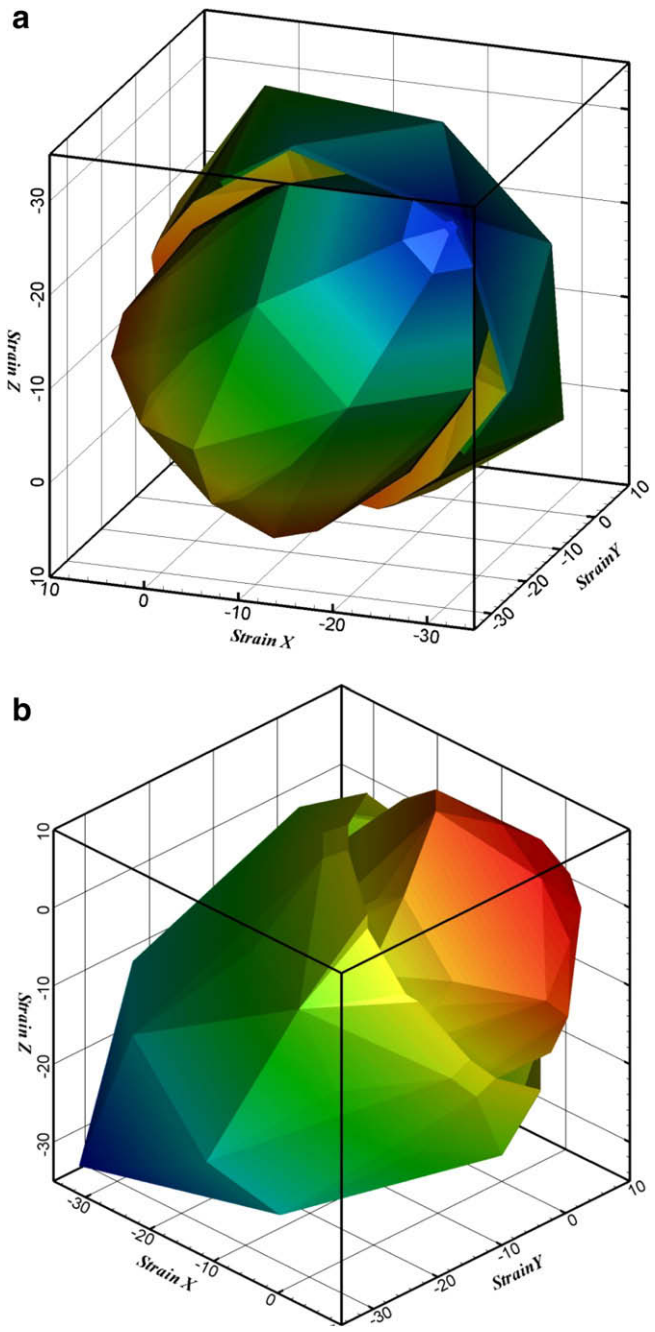

Fig. 9. The validity surfaces for 1372 and 4000-atom specimens. The inner surface belongs to the larger specimen. For better representation the outer surface is cut on its (a) meridian plane (b) π-plane.

Table 1
Constants of the validity surface Eq. (14).

Specimen	A	B	C	D
1372-atom	0.444	0.248	1.432	0.772
4000-atom	1.222	0.211	1.241	0.575

$\rho = \sqrt{\gamma_x^2 + \gamma_y^2 + \gamma_z^2}$ and the parameters m_0 and $r(\cos(\theta))$ are defined as

$$m_0 = 3\frac{e}{e+1}\frac{\varepsilon_c^2 - \varepsilon_t^2}{\varepsilon_c \varepsilon_t}$$

$$r(cos(\theta)) = \frac{4(1-e^2)cos^2(\theta) + (2e-1)^2}{2(1-e^2)cos(\theta) + (2e-1)\sqrt{4(1-e^2)cos^2(\theta) + 5e^2 - 4e}} \quad (15)$$

where ε_t is the limit uniaxial tensile strain, ε_c the limit uniaxial compressive strain and ε_b the limit equi-biaxial strain. In above relations, $\theta = \frac{1}{3}\arccos\left(\frac{3\sqrt{3}}{2}\frac{J_3}{J_2}\right)$ with and $J_2 = \rho^2/2$, $J_3 = \gamma_x\gamma_y\gamma_z$, and $e = (1+\alpha)/(2-\alpha)$ with α defined as

$$\alpha = \frac{\varepsilon_t}{\varepsilon_b}\frac{\varepsilon_b^2 - \varepsilon_c^2}{\varepsilon_c^2 - \varepsilon_t^2}$$

Eq. (14) is similar to the damage-plastic model proposed by Grassl and Jirasek (2006) for concrete failure. The constants variables in the Eq. (14) are provided in Table 1. In multi-scale simulation, it is not necessary to consider the finer scale to enrich the model while the nodal strains are within this surface.

Since the procedure used in the molecular dynamics is based on the displacement-control approach, the samples with distinctly different deformations broke down in a similar stress state. In fact, although we utilized different deformation paths in three-dimensional tensile tests, the corresponding break points are almost identical. In order to obtain the validity surface in the stress domain, simulations should be carried out by exerting the value of stress to the boundaries of the cubic specimens, i.e. performing the force control molecular dynamics experiments.

5. Conclusion

In the present paper, the 3D molecular dynamics simulation was performed at zero temperature to investigate the stability and size-dependency of a well-known Cauchy–Born hypothesis. The MD simulation was applied to lead the system to a configuration which locally minimizes the potential energy of the system, and to reflect the concept of CB hypothesis as a rough guess for the real deformation of crystalline structures. Explorations were made for the cubic gold specimen. In order to model the real metallic behavior at nano-scale structures, the Sutton–Chen many-body potential was utilized by calculating the strain energy density and the force field in the continuum and molecular models. To determine the failure point of CB hypothesis two failure criteria were introduced in the strain and stress domains. It is shown that the overall behavior of the system is size-independent before the break point in most cases. The failure point decreases with the increase of the size of samples. It is illustrated that in compressive loading, the CB failure does not correspond to the material yield point of the specimen. This phenomenon was investigated by unloading the specimen from different break points and it was disclosed that the CB failure occurs before the initiation of the plastic regime. It was shown that in compressive loading the specimen may undergo the inhomogeneous recoverable deformation. Furthermore, a hysteresis phenomenon was observed in unloading process, which is caused due to irreversibility of NVT simulations and is exacerbated by entanglement in a local minimal point at zero temperature. By implementation of three-dimensional deformation paths, the validity surfaces were obtained in strain space for different samples, and the equation of validity surfaces were derived. As a practical guideline, it has been illustrated that the CB hypothesis is quite acceptable in the regions that the principal strains are almost uniform within the proposed validity surface. It is numerically shown that the surface shrinks as the size of specimen increases.

References

Ackland, G.J., Vitek, V., 1990. Many-body potentials and atomic-scale relaxations in nobel-metal alloys. Physical Review B 41, 10324–10333.
Allen, M.P., Tildesley, D.J., 1987. Computer Simulation of Liquids. Clarendon Press, Oxford.

Belytschko, T., Liu, W.K., Moran, B., 2000. Nonlinear Finite Elements for Continua and Structures. Wiley, New York.
Berendsen, H.J.C., Postma, J.P.M., van Gunsteren, W.F., DiNola, A., Haak, J.R., 1984. Molecular dynamics with coupling to an external bath. Journal of Chemical Physics 81, 3684–3690.
Born, M., Huang, K., 1962. Dynamical Theory of Crystal Lattices, first ed. Oxford University Press.
Braides, A., Dal Maso, G., Garroni, A., 1999. Variational formulation of softening phenomena in fracture mechanics: the one-dimensional case. Archive for Rational Mechanics and Analysis 146, 23–58.
Dingreville, R., Qu, J., Cherkaoui, M., 2005. Surface free energy and its effect on the elastic behavior of nano-sized particles, wires and films. Journal of the Mechanics and Physics of Solids 53, 1827–1854.
Domke, J., Radmacher, M., 1998. Measuring the elastic properties of thin polymer films with the atomic force microscope. Langmuir 14, 3320–3325.
Duana, H.L., Wanga, J., Huanga, Z.P., Karihaloob, B.L., 2005. Size-dependent effective elastic constants of solids containing nano-inhomogeneities with interface stress. Journal of the Mechanics and Physics of Solids 53, 1574–1596.
Elliott, R.S., Triantafyllidis, N., Shaw, J.A., 2006. Stability of crystalline solids I: continuum and atomic lattice considerations. Journal of the Mechanics and Physics of Solids 54, 161–192.
Ericksen, J.L., 1984. The Cauchy Born Hypotheses for Crystals, Phase Transformations and Material Instabilities in Solids. In: Gurtin, M.E. (Ed.). Academic Press, pp. 61–77.
Fleck, N.A., Hutchinson, J.W., 1993. A phenomenological theory for strain gradient effects in plasticity. Journal of the Mechanics and Physics of Solids 41, 1825–1867.
Friesecke, G., Theil, F., 2002. Validity and failure of the Cauchy–Born hypothesis in a two-dimensional mass-spring lattice. Journal of Nonlinear Science 12, 445–478.
Gao, H., Huang, Y., 2003. Geometrically necessary dislocation and size-dependent plasticity. Scripta Materialia 48, 113–118.
Grassl, P., Jirasek, M., 2006. Damage-plastic model for concrete failure. International Journal of Solids and Structures 43, 7166–7196.
Guo, Y., Zhuang, Z., Li, X.Y., Chen, Z., 2007. An investigation of the combined size and rate effects on the mechanical responses of FCC metals. International Journal of Solids and Structures 44, 1180–1195.
He, L.H., Lim, C.W., Wu, B.S., 2004. A continuum model for size-dependent deformation of elastic films of nano-scale thickness. International Journal of Solids and Structures 41, 847–857.
Horstemeyer, M.F., Baskes, M.I., Plimpton, S.J., 2001. Computational nano scale plasticity using embedded atom potentials. Theoretical and Applied Fracture Mechanics 37, 49–98.
Huang, X., Pelegri, A.A., 2007. Finite element analysis on nanoindentation with friction contact at the film/substrate interface. Composites Science and Technology 67, 1311–1319.
Khoei, A.R., Abdolhosseini Qomi, M.J., Kazemi, M.T., Aghaei, A., 2009. An investigation on the validity of Cauchy–Born hypothesis using Sutton–Chen many-body potential. Computational Materials Science 44, 999–1006.
Liu, W.K., Karpov, E.G., Zhang, S., Park, H.S., 2004. An introduction to computational nanomechanics and materials. Computer Methods in Applied Mechanics and Engineering 193, 1529–1578.
Malvern, L.E., 1968. Introduction to the Mechanics of a Continuous Medium. Prentice Hall. MASS Software, http://www.nano-mass.com.
Miller, R.E., Shenoy, V.B., 2000. Size-dependent elastic properties of nanosized structural elements. Nanotechnology 11, 139–147.
Park, H.S., Liu, W.K., 2004. An introduction and tutorial on multiple-scale analysis in solids. Computer Methods in Applied Mechanics and Engineering 193, 1733–1772.
Rafii-Tabar, H., 2000. Modelling the nano-scale phenomena in condensed matter physics via computer-based numerical simulations. Physics Reports 325, 239–310.
Rapaport, D.C., 1995. The Art of Molecular Dynamics Simulation. Cambridge University Press.
Salacuse, J.J., Denton, A.R., Egelstaff, P.A., 1996. Finite-size effects in molecular dynamics simulations: static structure factor and compressibility. I. Theoretical method. Physical Review E 53, 2382–2389.
Sauer, R.A., Li, S., 2007. An atomistically enriched continuum model for nanoscale contact mechanics and its application to contact scaling. Journal of Nanoscience and Nanotechnology 8, 1–17.
Sharma, P., Ganti, S., Bhate, N., 2003. Effect of surfaces on the size-dependent elastic state of nano-inhomogeneities. Applied Physics Letters 82, 535–537.
Shen, S., Atluri, S.N., 2004. Atomic-level stress calculation and continuum-molecular system equivalence. Computer Modeling in Engineering and Sciences 6, 91–104.
Srivastava, D., Atluri, S.N., 2002. Computational nanotechnology: a current perspective. Computer Modeling in Engineering and Sciences 3, 531–538.
Steinmann, P.A., Elizondo, A., Sunyk, R., 2007. Studies of validity of the Cauchy–Born rule by direct comparison of continuum and atomistic modeling. Modeling and Simulation in Material Science and Engineering 15, 271–281.
Streitz, F.H., Cammarata, R.C., Sieradzki, K., 1994. Surface-stress effects on elastic properties. II. Metallic multilayers. Physical Review B 49, 10707–10716.
Subramaniyan, A.K., Sun, C.T., 2008. Continuum interpretation of Virial stress in molecular simulations. International Journal of Solids and Structures 45, 4340–4346.
Sunyk, R., Steinmann, P., 2003. On higher gradients in continuum-atomistic modelling. International Journal of Solids and Structures 40, 6877–6896.
Sutton, A.P., Chen, J., 1990. Long-range Finnis–Sinclair potentials. Philosophical Magazine 61, 139–146.
Tadmor, E.B., Ortiz, M., Phillips, R., 1996. Quasicontinuum analysis of defects in solids. Philosophical Magazine A 73, 1529–1563.
Wang, J., Yip, S., Phillpot, S., Wolf, D., 1993. Crystal instabilities at finite strain. Physical Review Letters 71, 4182–4185.
Wong, E., Sheehan, P.E., Lieber, C.M., 1997. Nanobeam mechanics: elasticity, strength, and toughness of nanorods and nanotubes. Science 277, 1971–1975.
Xiao, S.P., Belytschko, T., 2004. A bridging domain method for coupling continua with molecular dynamics. Computer Methods in Applied Mechanics and Engineering 193, 1645–1669.
Xiao, S., Yang, W., 2006. Temperature-related Cauchy–Born rule for multiscale modeling of crystalline solids. Computational Material Science 37, 374–379.
Yoshimoto, K., Papakonstantopoulos, G.J., Lutsko, J.F., de Pablo, J.J., 2005. Statistical calculation of elastic moduli for atomistic models. Physical Review B 71, 184108.
Zhou, L.G., Huang, H., 2004. Are surfaces elastically softer or stiffer? Applied Physics Letters 84, 1940–1942.
Zimmerman, J.A., Webb, E.B., Hoyt, J.J., Jones, R.E., Klein, P.A., Bammann, D.J., 2004. Calculation of stress in atomistic simulation. Modelling and Simulation in Materials Science and Engineering 12, 319–332.